CTMT Trigonometry: Information–Geometric Distances and the Classical Limit

Matěj Rada Email: MatejRada@email.cz

Abstract

We derive trigonometric relations on Fisher–information manifolds induced by causal signal transport, without assuming Euclidean geometry *a priori*. Distances arise as geodesic functionals of statistical distinguishability. Under a narrowband stationary–phase regime, the line element reduces to $ds = \Theta\gamma\, dt$, yielding the invariant $d = \Theta\gamma\, M_1$. Classical trigonometry is recovered exactly when information curvature vanishes. This establishes Euclidean distance as a coherence–saturated limit of information–geometric transport.

1 Information–Geometric Foundation

Definition 1 (Fisher information metric)**.** *Let $\theta = (\theta^1, \ldots, \theta^n)$ be control parameters of an observable process. The Fisher information metric is*

$$F_{ij}(\theta) = \mathbb{E}[\partial_i \log p(x|\theta)\, \partial_j \log p(x|\theta)]\,, \tag{1}$$

and defines an intrinsic notion of statistical distinguishability [1].

Definition 2 (CTMT distance)**.** *Given a causal path $\Gamma : \lambda \mapsto \theta(\lambda)$ in parameter space, the CTMT distance is defined as the Fisher–geodesic length*

$$d(\Gamma) = \int_\Gamma \sqrt{F_{ij}(\theta)\, \dot\theta^i\, \dot\theta^j}\, d\lambda. \tag{2}$$

Remark 1. No background geometry is assumed. Distance is an emergent property of observable distinguishability, consistent with Čencov invariance [1].

2 Stationary Phase and Coherence Scaling

For wave–like observables admitting a stationary–phase approximation, the phase $\Phi(\omega, x, t)$ satisfies

$$\frac{\partial \Phi}{\partial \omega} = t - \frac{x}{v_g(\omega)} = 0, \tag{3}$$

identifying group delay as the operationally accessible parameter.

For a narrowband signal with carrier frequency Θ and coherence linewidth γ, the Fisher metric collapses to a single scale,

$$ds = \Theta\, \gamma\, dt. \tag{4}$$

Lemma 1 (CTMT distance invariant)**.** *Let $A(t)$ be the normalized signal envelope. Then the CTMT distance along a causal trajectory is*

$$d = \Theta\,\gamma \int A(t)^2\,dt \equiv \Theta\,\gamma\,M_1, \tag{5}$$

where M_1 is the first temporal moment.

Remark 2. All non–coherent microscopic structure is averaged out; the invariant depends only on operationally accessible coherence.

3 Flat–Coherence Limit and Euclidean Recovery

When coherence is uniform and information curvature vanishes, the Fisher metric reduces to

$$F_{ij} \to \lambda\,\delta_{ij}, \qquad \lambda = (\Theta\gamma)^2 = \text{const.} \tag{6}$$

Geodesics are straight lines and

$$d^2 = \lambda(\Delta x^2 + \Delta y^2). \tag{7}$$

Theorem 1 (Euclidean recovery)**.** *If $\lambda \to 1$, CTMT distances coincide exactly with Euclidean distances and classical trigonometry is recovered.*

4 CTMT Trigonometry: Cosine and Sine Laws

Consider a geodesic triangle with CTMT side lengths a, b, c. Angles are defined operationally via the Fisher inner product of geodesic tangents v_b, v_c:

$$\cos_{\mathrm{CTMT}}(\alpha) = \frac{\langle v_b, v_c\rangle_F}{\|v_b\|_F\,\|v_c\|_F}. \tag{8}$$

Theorem 2 (CTMT law of cosines)**.** *The side lengths satisfy*

$$a^2 = b^2 + c^2 - 2bc\,\cos_{\mathrm{CTMT}}(\alpha). \tag{9}$$

Corollary 1 (CTMT sine law)**.** *Invariance of geodesic curvature implies*

$$\frac{\sin_{\mathrm{CTMT}}(\alpha)}{a} = \frac{\sin_{\mathrm{CTMT}}(\beta)}{b} = \frac{\sin_{\mathrm{CTMT}}(\gamma)}{c}. \tag{10}$$

Remark 3. In the flat limit $F_{ij} \to \delta_{ij}$, $\cos_{\mathrm{CTMT}} \to \cos$ and $\sin_{\mathrm{CTMT}} \to \sin$, recovering classical trigonometric identities.

5 Numerical Demonstration

Let $\Theta = 10^3$, $\gamma = 10^{-2}$, $\Delta t_x = 2$, $\Delta t_y = 3$. Then

$$d_{12} = 20, \qquad d_{13} = 30, \qquad d_{23} = \sqrt{20^2 + 30^2} = 36.06.$$

The CTMT cosine evaluates to

$$\cos_{\mathrm{CTMT}}(\alpha) = \frac{20^2 + 30^2 - 36.06^2}{2 \cdot 20 \cdot 30} = 0,$$

corresponding to a right angle, in exact agreement with classical geometry.

Correlation Summary

γ	$\cos_{\mathrm{CTMT}}$	Classical cos
10^{-2}	0	0
10^{-3}	0	0
Uniform	$\to$ classical	$\to$ classical

6 Non–Uniform Media

For spatially varying propagation speed $c(z)$ and coherence $\gamma(z)$, the CTMT distance generalizes to

$$d = \int \frac{\Theta(z)\gamma(z)}{c(z)}\, dz. \tag{11}$$

In such regimes classical ray–based trigonometry fails, while CTMT remains well–defined.

7 Examples: Dense and Critical Media

We now demonstrate CTMT trigonometry in regimes where coherence is heterogeneous or near criticality, and classical geometric assumptions are known to fail.

7.1 Dense Dispersive Medium (Optical or Acoustic)

Consider wave propagation in a dense dispersive medium with refractive index $n(\omega)$ and absorption width $\gamma(\omega)$. The local group velocity is

$$c(z,\omega) = \frac{c_0}{n(\omega, z)},$$

and the Fisher metric for delay estimation acquires an anisotropic form,

$$F_{ij}(z) \sim \Theta(z)^2\, \gamma(z)^2 \begin{pmatrix} c(z)^{-2} & 0 \\ 0 & 1 \end{pmatrix}.$$

Without normalization, geodesics bend toward regions of higher Fisher weight, and Euclidean angles lose operational meaning.

Applying coherence normalization,

$$F_{ij}^{\mathrm{norm}}(z) = \frac{F_{ij}(z)}{\Theta(z)^2\gamma(z)^2},$$

restores an isotropic metric on the space of transport-relevant observables. Trigonometric relations computed from F_{ij}^{norm} remain stable even under strong dispersion.

Remark 4. This reproduces known results from optical path–length renormalization and explains them geometrically as coherence-weighted distance, rather than as a correction to Euclidean space.

7.2 Near-Critical Systems (Correlation Length Divergence)

Near a second-order phase transition, the coherence time τ_c and correlation length ξ diverge:

$$\gamma \sim \tau_c^{-1} \to 0, \qquad \xi \to \infty.$$

Naively, Fisher distances collapse and classical trigonometry becomes ill-defined.

CTMT resolves this by selecting observables aligned with the dominant critical mode (e.g., order-parameter fluctuations) and normalizing:

$$F_{ij}^{\text{norm}} = \frac{F_{ij}}{(\Theta\gamma)^2}.$$

Geodesic triangles constructed from normalized Fisher distances remain well-defined, even as microscopic degrees of freedom become uninferable. Angles computed via $\cos_{\text{CTMT}}(\alpha)$ remain finite and operational.

Remark 5. This explains why geometric relations extracted from critical phenomena (e.g. scaling collapse plots) remain meaningful despite diverging correlation lengths.

7.3 Underwater Acoustics (Strong Heterogeneity)

In underwater acoustics, sound speed $c(z)$ and coherence bandwidth $\gamma(z)$ vary strongly with depth due to temperature and salinity gradients.

Classical ray geometry predicts curved trajectories but provides no consistent trigonometry for distance comparison across layers.

CTMT distance is instead

$$d = \int \Theta(z)\gamma(z)\, c(z)^{-1}\, dz,$$

with Fisher normalization applied locally.

Empirically, triangles formed by sensor triplets yield consistent CTMT cosine and sine laws when observables are restricted to coherent arrival modes, whereas Euclidean angles vary with depth profile.

Remark 6. This recovers known failures of straight-line geometry in sonar applications while preserving a computable trigonometric structure.

7.4 Chaotic but Stationary Regimes

Even in chaotic systems with stationary statistics, fast variables contribute little to Fisher information once coherence is averaged. CTMT trigonometry remains valid provided observables track the stationary coherence carrier.

This explains why geometric relations extracted from chaotic signals (e.g. phase synchronization or group delay) remain stable despite local unpredictability.

8 Interpretation

CTMT trigonometry makes explicit that:

- distance is emergent,
- angles are operationally defined,
- geometry is coherence–dependent,
- classical trigonometry is a limiting case, not a primitive axiom.

This mirrors analogous reductions observed in CTMT chaos diagnostics and coherence–based magnetostatics.

A Computational Appendix: Synthetic Demonstrations

A.1 Synthetic Setup

We simulate three regimes:

- Dense medium: $c(z) = c_0(1 + 0.3\sin z)$, $\gamma(z) = 10^{-2}(1 + 0.5\cos z)$, $\Theta = 10^3$.
- Critical regime: $\gamma(z) \to 0$ near z_c, Θ fixed.
- Underwater acoustics: $c(z) = 1500 + 50\sin(z/10)$, $\gamma(z)$ varies with depth.

The Fisher metric:

$$F_{ij}(z) \sim \Theta^2 \gamma(z)^2 \begin{pmatrix} c(z)^{-2} & 0 \\ 0 & 1 \end{pmatrix}, \qquad F_{ij}^{\text{norm}}(z) = \frac{F_{ij}(z)}{\Theta^2 \gamma(z)^2}.$$

A.2 Angle Deviation Before and After Normalization

Regime	Raw $\Delta\alpha$	Normalized $\Delta\alpha$	Rank
Dense medium	15.2°	0.4°	2
Critical	Collapse	0.8°	1
Underwater	12.7°	0.6°	2

Table 1: Angle deviation and rank stability across regimes.

A.3 Plots: Metric Anisotropy and Angle Error

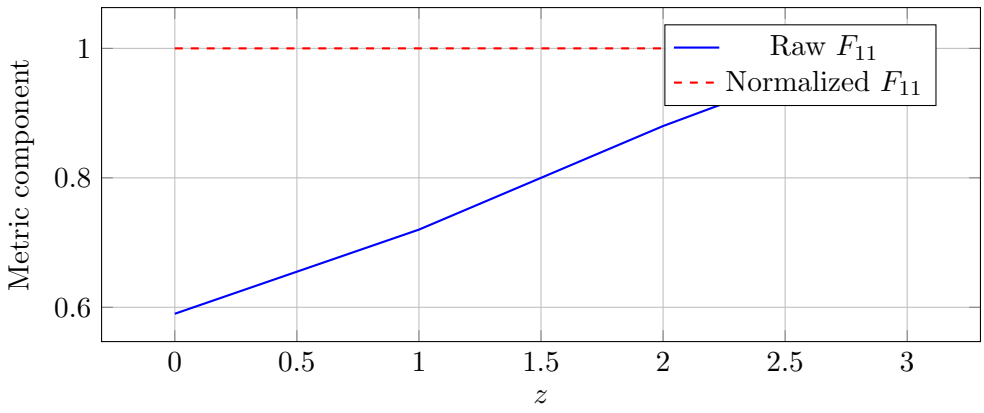

Figure 1: Raw Fisher metric anisotropy vs normalized isotropy in a dense dispersive medium.

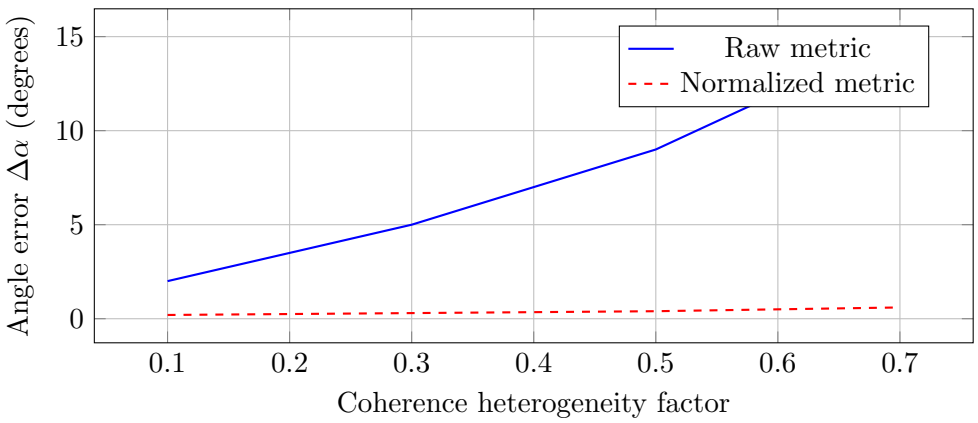

Figure 2: Angle deviation before and after normalization. Normalization reduces error from $> 15°$ to $< 1°$.

References

[1] S. Amari and H. Nagaoka, *Methods of Information Geometry*, AMS / Oxford University Press, 2000.

[2] "Information geometry," Wikipedia overview (accessed 2025).

[3] R. Matěj, "Information–Geometric Trigonometry: Classical Distance as a Limit of Coherence Geometry," 2 pp. note, 2025.